Published in final edited form as:
*Nanotoxicology*. 2012 December ; 6: 837–846. doi:10.3109/17435390.2011.625131.

# Serum proteins prevent aggregation of $Fe_2O_3$ and ZnO nanoparticles

**Mark A. Wells**[1], **Aamir Abid**[1], **Ian M. Kennedy**[1], and **Abdul I. Barakat**[1,2]

[1]Department of Mechanical and Aerospace Engineering, University of California, Davis CA, USA

[2]Hydrodynamics Laboratory (LadHyX), CNRS UMR7646, Ecole Polytechnique, France

## Abstract

Aggregation of metal oxide nanoparticles in aqueous media complicates interpretation of *in vitro* studies of nanoparticle–cell interactions. We used dynamic light scattering to investigate the aggregation dynamics of iron oxide and zinc oxide nanoparticles. Our results show that iron oxide particles aggregate more readily than zinc oxide particles. Pretreatment with serum stabilises iron oxide and zinc oxide nanoparticles against aggregation. Serum-treated iron oxide is stable only in pure water, while zinc oxide is stable in water or cell culture media. These findings, combined with zeta potential measurements and quantification of proteins adsorbed on particle surface, suggest that serum stabilisation of iron oxide particles occurs primarily through protein adsorption and resulting net surface charge. Zinc oxide stabilisation, however, also involves steric hindrance of particle aggregation. Fluid shear at levels used in flow experiments breaks up iron oxide particle aggregates. These results enhance our understanding of nanoparticle aggregation and its consequences for research on the biological effects of nanomaterials.

### Keywords

Metal oxide nanoparticles; particle aggregation; particle aging; dynamic light scattering; zeta potential; fluid shear

## Introduction

Metal oxide nanoparticles have come under scrutiny as an environmental and occupational health hazard. These particles are ubiquitous in the urban environment, generated by sources such as internal combustion engines, industrial furnaces and welding and fabrication processes. Unlike larger particles, inhaled nanoparticles can reach the alveoli and may enter the systemic circulation (Nemmar et al. 2001; Oberdörster et al. 2002). This could account for extrapulmonary effects of particle inhalation, including the widely observed relationship between episodes of elevated particulate air pollution and sudden cardiac death (Dockery 2001).

*In vitro* studies of nanoparticle–cell interactions play an essential role in understanding the pathology of nanoparticle exposure. Several injurious effects have been demonstrated, including expression of inflammatory cytokines (Gojova et al. 2007), DNA damage



Correspondence: Prof. Abdul I. Barakat, Department of Mechanical and Aerospace Engineering, University of California, Davis, One Shields Avenue, Davis, CA 95616. Tel: +530 754 9295. Fax: +530 752 4158. abarakat@ucdavis.edu.

Declaration of interest
The authors report no conflicts of interest. The authors alone are responsible for the content and writing of the paper.

(Karlsson et al. 2008), membrane leakage and loss of mitochondrial function (Jeng & Swanson 2006).One mechanism commonly invoked to explain these effects is catalytic free radical production, with iron and other transition metals acting as electron carriers (Gilmour et al. 1996; Lin et al. 2009).

One significant limitation of *in vitro* studies is that metal oxide particles aggregate rapidly when suspended in aqueous media. While nanoparticles produced for industrial or medical use (such as paint pigments and magnetic resonance imaging (MRI) contrast agents) are usually stabilised with surfactants or hydrophilic coatings, flame-generated ambient particles are not. Aggregation changes the effective particle size, which may alter the particle/cell interaction by means such as promoting or inhibiting endocytosis (Pratten & Lloyd 1986) or limiting the surface area available to catalyse reactions such as free radical production (Thomassen et al. 2010). Aggregation also affects particle transport in fluid environments and hence the dose of material delivered to the cells.

Accordingly, research in nanotoxicology increasingly recognises the importance of measuring the extent of particle aggregation in the test system (Meißner et al. 2009; Schulze et al. 2008). A recent study characterised the effect of ionic strength, pH and particle surface chemistry on aggregation of titania nanoparticles and quantum dots in deionised (DI) water (Jiang et al. 2009).

It is expected that aggregation rates of nanoparticles can be altered by surface adsorption of biomolecules. To address more biologically relevant conditions, we investigated the aggregation and sedimentation behaviour of flame-generated iron oxide and zinc oxide nanoparticles suspended in cell culture media. Additional factors considered were the presence of serum proteins and exposure to fluid shear stress at a typical physiological level.

## Materials and methods

### Nanoparticle synthesis

Nanoparticles were produced as described previously (Gojova et al. 2007). Briefly, a hydrogen diffusion flame was seeded with the vapour of either iron pentacarbonyl (99.5%; Alfa Aesar, Ward Hill, MA, USA) or elemental zinc (99.999%; Alfa Aesar). Particles of $\gamma$-$Fe_2O_3$ (maghemite) or zinc oxide were collected on a cold finger. The nanoparticle morphologies were investigated using a Phillips CM-12 transmission electron microscope operated at 120 kV. Nanoparticles were suspended in DI water and deposited on a 400 mesh copper TEM (transmission electron microscopy) grid with a carbon/formvar film (Ted Pella Inc., Redding, CA, USA, Prod # 01754-F); excess liquid was wicked away.

### Dynamic light scattering

Particle size measurements were performed using a BIC 90Plus dynamic light scattering (DLS) instrument (Brookhaven Instruments, Holtsville, NY, USA). For each measurement, data were collected for 30 min and a single autocorrelation curve was analysed. The baseline for autocorrelation was set by identification of a zero-slope region of the curve. The following properties were calculated by the 90Plus software:

- Effective diameter: The particle diameter corresponding to the first cumulant of the correlation curve. This is equivalent to the size of uniform particles that would best approximate the observed correlation behaviour. For multimodal distributions, it is weighted roughly by scattering intensity.
- Count rate: The average number of photon detection events per second during the measurement interval.

- Number-weighted particle size distribution: The histogram of particle diameters determined by the 90Plus software to approximate the correlation curve. The bins of the histogram are logarithmically spaced, and the particle counts in each bin are normalised to give the largest bin a count of 100. We denote this diameter as "peak". The number-weighted average ("NWA") diameter was calculated from the distribution using a Perl script.

We expected count rate to function as an indicator of particle density in the beam path. This was validated using serial dilutions of a nearly monodisperse polystyrene particle standard ("Nanosphere", Duke Scientific Corp, Palo Alto, CA, USA) as shown in Figure 1. Over this range, the count rate was found to vary with particle concentration to the power of 0.91. This model correlates extremely well with the data ($r^2 > 0.999$).

### Dispersion and recovery in deionised water

Particles were suspended in DI water at concentrations of 10 μg/ml (iron oxide) or 50 μg/ml (zinc oxide). These concentrations were chosen to achieve an initial signal intensity above 200,000 counts per second and no visible "halo" around the laser beam. Each sample was measured by DLS at three times: after diluting and gently mixing the suspension in the cuvette; after direct-contact sonication for 60 s using a Branson Sonifier 250 with micro tip and 24 h after sonication (with the sample kept at room temperature). Six independent samples were measured for each particle type, and the results (effective diameter and NWA diameter) were averaged.

### Serum treatment

Iron oxide or zinc oxide particles were suspended at 200 μg/ml in foetal calf serum (Gemini Bio-Products, West Sacramento, CA, USA) and mildly sonicated by immersion in a Cole-Parmer 8891 ultrasound bath for 10 min. The particles were then centrifuged at 10,000 rpm for 10 min (iron oxide) or 30 min (zinc oxide). The supernatant was removed and replaced with a diluent. The particles were re-suspended, sonicated and centrifuged two more times to remove free serum proteins, then re-suspended in the same diluent at 20 μg/ml. Serum-free controls were processed by the same procedure but with initial suspension in diluent instead of serum.

Zinc oxide particles proved resistant to centrifugation, despite having nearly the same bulk density as iron oxide, and some material was invariably lost during the washes. To ensure consistent particle concentration, the final suspension was placed into the instrument and its count rate was measured. This suspension was then diluted according to the ratio between its count rate and that of a reference suspension of 20 μg/ml zinc oxide in water.

### Short-term aging time course

Particles were treated with serum as above using four diluents: DI water, Dulbecco's phosphate buffered saline (PBS) without calcium or magnesium (Invitrogen, Carlsbad, CA, USA), endothelial cell basal medium-2 (EBM-2, Lonza, Basel, Switzerland) or complete endothelial cell growth medium-2 (EGM-2, Lonza) including 2% foetal calf serum. Serum-treated and serum-free samples were prepared using each diluent except EGM-2; particles were suspended in EGM-2 without serum treatment.

Within one day of preparation, each sample was dispersed with 60 s of direct-contact sonication. Particle size (effective diameter) and count rate were measured by DLS over intervals of 1 h for 12 h, with the first measurement starting immediately after sonication. During this time, the sample was left in the instrument to avoid mixing by external forces.

### Surface adsorbed protein quantification

Surface adsorbed proteins were quantified using the bicinchoninic acid (BCA) assay with bovine serum albumin as a calibration standard. Iron oxide and zinc oxide samples with and without serum pretreatment were prepared in four diluents (DI water, PBS, EBM-2 and EGM-2) as described above. In the case of complete media, the particles were not pretreated with serum. The particle concentrations were at 200 μg/ml. The absorption measurements ($\lambda$ = 560 nm) were performed on a SpectraMax M2 cuvette/microplate reader (Molecular Devices Inc., Sunnyvale, CA, USA) using the SOFTmax PRO software. Samples were probe sonicated before measurements and the measurements were made in triplicate. The adsorbed protein concentration was determined by subtracting the signal of uncoated bare particles from protein-coated particles in each of the diluents studied. Measurements of protein desorption were done on serum-pretreated iron oxide particles suspended in 0.5 M KCl solution using the BCA protein assay. The particles were centrifuged as described above and the concentration of protein in the supernatant was determined.

### Zeta potential

Zeta potential was measured by light scattering using a BIC ZetaPlus instrument (Brookhaven Instruments Corp., Holtsville, NY, USA). Particles were treated with and without serum as above using four diluents (DI water, PBS, EBM-2 and EGM-2). In the case of EGM-2 the particles were not pretreated with serum. The suspensions were dispersed with 60 s of probe sonication and immediately measured with the ZetaPlus instrument. At least three measurements were made in each case and the data were averaged.

### Fluid shear

Iron oxide particles were dispersed in water at 2 mg/ml by sonication then diluted to 50 μg/ml with complete EGM-2. An aliquot of this suspension (the static control) was placed in the DLS instrument and measured over intervals of 30 min for 4 h. The remaining suspension was circulated at 70 ml/min through a recirculating flow loop of tubing (ID = 3.1 mm) using a peristaltic pump. The estimated maximum shear stress in the tubing was 3.1 dyne/cm$^2$. At the end of this period, another aliquot was taken from the flow loop and measured by DLS for one 30-min interval.

In a variation on this experiment, the static control sample was measured once at the beginning of flow. After each hour of flow, a 1-ml aliquot was taken from the flow loop and measured for 30 min. After 4 h, the static control was measured again.

## Results

### Particle dispersion and recovery

Preliminary measurements with iron oxide and zinc oxide particles showed a highly polydisperse distribution, while TEM images (Figure 2) showed aggregates of 50–100 nm particles (after dehydration of the material). It is possible that the aggregation occurs during the drying of sample on the TEM grid and indeed DLS measurements show that the primary particle size is recovered after probe sonication as discussed below.

DLS was used to measure the aggregation state of the particles in suspension and to assess the effectiveness of sonic dispersion. Particle sizes before and after sonication for both iron oxide (10 μg/ml) and zinc oxide (50 μg/ml) are shown in Figure 3. The effective, peak and NWA diameters are shown. Effective diameter is inherently weighted by the scattering intensity of each particle, and therefore indicates the size of the largest objects present. Peak and NWA correspond more closely to the size of a “typical” particle.

### Short-term particle aging

Particles used in cell culture studies are necessarily submerged for several hours in culture medium containing salts, various small molecules and serum proteins or other macromolecules. The time-course experiment was designed to investigate the kinetics of aggregation and the influence of medium components.

Time courses were run with the particles suspended in water, PBS or EBM-2 (with and without serum pretreatment of the particles), and in complete endothelial cell medium with serum. Number-averaged diameter showed no significant trends. This is consistent with the dispersion/recovery results (showing very little change over the 24-h recovery period) and with the theory of particle aggregation which predicts catastrophic growth of the largest clusters by capturing primary particles. Therefore, only two measures are shown for the time courses: effective diameter and the average photon count rate reported by the instrument. Count rate was normalised to the count rate for the first hour.

The results for iron oxide are shown in Figure 4 where the bars represent consecutive 1-h time steps. All treatment conditions show a large increase in effective diameter and a decrease in scattering intensity, except for serum-treated particles in water. Figure 5 shows the same results for zinc oxide. Unlike iron oxide, these particles resisted aggregation in all serum-treatment conditions, as well as complete medium. For comparison, Table I shows average results at the final time point (12 h).

### Zeta potential

Zeta potential was measured in order to gain some insight into the mechanism of nanoparticle size stabilisation. A widely cited empirical rule holds that electrostatic stabilisation requires zeta potentials of at least ±30 mV (Berg et al. 2009; Bergman et al. 2008). Exceptions to this rule exist: Hang et al. (2009) reported electrostatic stabilisation of barite at ±15 mV. However, stability at low zeta potential more commonly implies some degree of steric stabilisation.

Zeta potential measurements in various diluents are shown in Figure 6. The isoelectric point for maghemite is 5.5 and that for zinc oxide is 8.8–9.8 (Kosmulski 2001). Consequently, in neutral pH solution, the zeta potential for iron oxide is negative and that for zinc oxide is positive. The potential of iron oxide in DI water was affected very little by serum treatment (change of −4.0 mV, less than the combined standard deviation of the two groups). On the other hand, zinc oxide in DI water showed a strong negative shift (−39.2 mV) consistent with the potent effect of serum in stabilising this material. The zeta potential for both iron oxide and zinc oxide in PBS, EBM-2 and EGM-2 (complete medium) is close to zero, indicating that the stability of the particles is not dominated by surface charge effects. The same is seen for particles pretreated with serum.

### Fluid shear

The fluid shear experiment was intended to simulate our system for exposing cells to physiologic levels of shear stress. We conjectured that the combination of shear stress (potentially breaking up soft aggregates) and continuous mixing (altering the dynamics of particle collisions) would affect the kinetics of aggregation. The conditions for this test were chosen to match our ongoing work on nanoparticle interaction with endothelial cells under flow.

Figure 7A shows the effective diameter measured by DLS for the static control in consecutive 30-min period and for the suspension circulated in the flow loop. The difference is readily apparent. The static samples reached an average effective diameter of 830 nm

during the first 30 min, increasing to 1550 nm over 4 h. Fluid shear completely negated the increase in diameter over this period, yielding an effective diameter of 620 nm at the end of the 4-h treatment. We attribute this effect to shear-induced breakup of aggregates. A detailed microscopic study by Tolpekin et al. (2004) showed that dispersions of weakly aggregating particles under shear flow reach a steady-state maximum size. The size limit is determined by the balance between aggregation and breakup events, and is highly sensitive to both particle concentration and shear rate.

This experiment does not indicate the time scale for shearing of aggregates. Therefore, we performed a complementary experiment in which effective diameter was measured over the duration of flow (Figure 7B). The results are approximated well by an exponential decay with a time constant of 1.1 h (dashed curve). Based on these results, we believe that the particles used in our cell culture system are probably minimally aggregated for most of the duration of a 6–24 h flow experiment.

### Surface proteins

A dynamic layer of protein or a corona is known to form around particles that are suspended in cell cultures (Lynch & Dwason 2008). The adsorbed proteins on a particle surface are expected to influence the interaction with living systems as well as the stability of the particles in solution. In order to quantify the amount of protein, if any, that gets adsorbed on iron oxide and zinc oxide nanoparticles, the BCA protein quantification assay was used. Figure 8 shows the concentration of protein adsorbed on iron oxide and zinc oxide in DI water and PBS. The concentrations are normalised by particle surface area values that were measured using the BET method in our previous work ($81 \pm 1$ and $20.8 \pm 0.2$ $m^2/g$ for iron oxide and zinc oxide, respectively; Gojova et al. 2007). There is a fourfold increase in protein concentration adsorbed on zinc oxide as compared with iron oxide suspended in DI water and PBS. In a study on protein adsorption on ceria nanoparticles, Patil et al. (2007) showed that particles having positive zeta potential adsorbed more protein than particles with negative zeta potential. Therefore, the stronger affinity of protein to zinc oxide can be attributed to the positive charge on the surface and explains the large shift in zinc oxide zeta potential on treatment with serum (Figure 6). Protein concentrations were also measured for particles suspended in cell culture media (EBM-2 and EGM-2), but the high background signal from protein in the media masked any signal that would have come from proteins adsorbed on particles and the data are not shown here.

## Discussion

### Dispersion and recovery behaviour

Iron oxide generally displayed a stronger tendency towards aggregation than zinc oxide. Sonication greatly reduced the effective, peak and NWA diameters for iron oxide, indicating that a large fraction of the primary particles were bound in aggregates. For zinc oxide, effective diameter decreased while peak and NWA were nearly unchanged. This suggests a relatively small fraction of aggregates mixed with a large population of primary particles. Particle size measurements one day after sonication suggested a partial return to the original state.

### Stabilisation by serum adsorption

A major finding of this study was that serum treatment of iron and zinc oxide particles stabilised them against aggregation and sedimentation. This was consistent with the behaviour of diverse inorganic materials such as titanium dioxide (Allouni et al. 2009; Vamanu et al. 2008; Meißner et al. 2009), tungsten carbide (Meißner et al. 2009) and fullerene (Deguchi et al. 2007). One possible stabilising agent in serum is albumin, which

carries a negative charge (around −20 elementary charges per molecule) at physiologic pH and therefore may stabilise the particles by imparting a net surface charge (Rezwan et al. 2004). Consistent with this, our serum-treated iron oxide particles were highly stable in DI water; however, we found that in an electrolyte solution, iron oxide was poorly stabilised and tended to aggregate. Zeta potential measurements showed virtually no change in the surface charge of these particles in PBS, EBM-2 and EGM-2. However, high salt concentrations can modify the structure of serum proteins adsorbed on the particle surface (Norde & Giacomelli 2000) and possibly influence the protein packing on the surface, diminishing their stabilising effect. It should be noted that due to the lot-to-lot variability in composition of serum used in cell culture studies, we confined our conclusions here to the effect of serum proteins in general rather than to particular proteins that may be present in serum.

Proteins that were desorbed in high salt solution were measured by separating particles from the solution by ultra-centrifugation. The protein concentration was 6 ± 0.1 mg/ml. By comparison, we measured 30 μg/ml of proteins in the particles suspended in DI water. It is therefore apparent that some proteins remained attached to the nanoparticles. Aggregation of iron oxide nanoparticles in PBS, EBM-2 and EGM-2 can result in diminished protein coating and reduced stability. An additional complicating factor is the experimental evidence that extracellular proteins may limit the dispersal of biogenic zinc sulfide nanoparticles (Moreau et al. 2007). A similar effect on nanoparticles used in the present study cannot be excluded.

DLS data showed that serum-treated zinc oxide remained stable even in electrolyte solutions. Figure 8 shows clearly that zinc oxide adsorbs significantly more protein than iron oxide due to the positive surface charge at physiologic pH (Patil el al. 2007). We propose that the zinc oxide particles are stabilised not only by surface charge, but by steric interference between their dense protein coats. From the results of Horie et al. (2009) who used 10 mg/ml of nanoparticles suspended in DMEM (Dulbecco's Modified Eagle Medium) with serum, the amount of adsorbed protein was approximately 0.05 mg/mg (protein/particles) for iron oxide and 0.12 mg/mg for zinc oxide. These equate to surface densities of 1.1 and 2.4 mg/m$^2$, or (for a 70 kDa protein) mean centreto-centre distance between protein molecules of 11 nm on iron oxide and 7.8 nm on zinc oxide. Since an albumin molecule has a hydrodynamic diameter of ~6 nm at physiologic pH (Luik et al. 1998), steric protection by albumin at this density is plausible.

## Consequences for cell culture studies

Uncoated metal oxide particles will aggregate within the time scale of a typical cell culture experiment. Aggregation may influence the nanoparticle–cell interaction in several ways. For example, effects dependent on the particle's free surface (such as free radical production) will likely diminish as particles aggregate. Conversely, phagocytosis appears to be more efficient for aggregates than for single particles (Geiser et al. 2008). Consistent with this, our previous study using endothelial cells (Gojova et al. 2007) showed large masses of iron oxide in intracellular vesicles. If desired, the effects of particle aggregation could be readily observed by allowing a pre-aging period between sonication and introduction to the cells.

Another area of concern is the effect of sedimentation on particle delivery to the cells. In the iron oxide/complete medium case, more than 75% of the suspended material was removed by sedimentation within 12 h. In a typical adherent cell culture system with the cells facing upward, all of this material will be deposited on the cell surface. Consequently, a bulk concentration of, for example, 1 μg/ml does not imply that 1 μg/ml of material will be available to the cells by diffusion. The local concentration may be significantly higher.

Finally, the effect of fluid shear on particle aggregation may act as a confounding factor in studies combining nanoparticle exposure with fluid flow. In a cell culture experiment, simply comparing flow with static conditions ignores the dramatic effect of flow on cluster size. A more exact control might involve, for example, externally circulating the particle suspension and slowly exchanging it with the media in contact with the cells.

### Implications for nanoparticle toxicology

Lynch & Dwason (2008) proposed that adsorption of a normally water-soluble protein, such as albumin, to a hydrophobic surface may unfold the protein. For example, Norde & Giacomelli (2000) found that adsorption to, and release from, polystyrene nanospheres altered the secondary structure of bovine serum albumin, while hydrophilic silica particles had no effect. We conjecture that protein misfolding in this manner may inactivate enzymatic or signalling functions of the protein, provoke an immune response against the altered structure or promote aggregation of the protein. To our knowledge, no specific pathology by this mechanism has been shown. There are a handful of reports of nanoparticle-induced protein aggregation in artificial environments (Linse et al. 2007; Wu et al. 2008), but as yet no demonstration of the effect *in vivo*.

Zinc oxide nanoparticles are known to be cytotoxic in culture and systemically toxic by inhalation. Whether the mechanism of toxicity is free radical production, soluble zinc release or some other process, the high specific surface area of these particles is likely to play a role. Additionally, their small size and high protein-binding capacity may enable them to avoid pulmonary macrophages and pass through the epithelium, entering the interstitial space or even the bloodstream. The comparison with titanium oxide is suggestive: inhaled titanium oxide provokes relatively little macrophage activity in the lungs (Driscoll et al. 1991) but alters microvascular signalling in skeletal muscle (Nurkiewicz et al. 2009), implying escape into the systemic circulation. A study by Deng et al. (2009) found that the specific serum proteins adsorbed by zinc and titanium oxides differ greatly. Notably, zinc oxide adsorbs abundant IgM and IgA, which the authors suggest may provoke cytokine release and neutrophil recruitment. Silica, by contrast, binds relatively little immunoglobulin of any type and causes lung injury through an unrelated mechanism.

## Conclusions

In conclusion, the present results indicate that iron oxide nanoparticles aggregate more readily than zinc oxide particles and that pretreatment with serum stabilises both types of particles against aggregation. Serum stabilisation of iron oxide particles occurs primarily through the effect of protein adsorption on surface charge whereas zinc oxide stabilisation also involves steric hindrance. These findings enhance our understanding of nanoparticle aggregation and its consequences for research on the effects of nanomaterials on cells.

## Acknowledgments

We are grateful to Dr. Marjorie Longo (Department of Chemical Engineering and Materials Science, UC Davis) for the use of particle sizing equipment, Dr. Thomas Young (Civil and Environmental Engineering, UC Davis) for the use of BIC ZetaPlus instrument and Will Bernt (Particle Characterisation Laboratories, Novato, CA, USA) for training and technical advice. Although the research described in the article has been funded in part by the United States Environmental Protection Agency through grant RD-83241401-0 to the University of California, Davis, it has not been subject to the Agency's required peer and policy review and therefore does not necessarily reflect the views of the Agency and no official endorsement should be inferred. This publication was made possible in part by grant number 5 P42 ES004699 from the National Institute of Environmental Health Sciences (NIEHS), NIH and the contents are solely the responsibility of the authors and do not necessarily represent the official views of the NIEHS, NIH. This work was funded in part by an endowment in Cardiovascular Cellular Engineering from the AXA Research Fund.

## References


Allouni ZE, Cimpan MR, Høl PJ, Skodvin T, Gjerdet NR. Agglomeration and sedimentation of TiO2 nanoparticles in cell culture medium. Coll Surf B. 2009; 68:83–87.

Berg JM, Romoser A, Banerjee N, Zebda R, Sayes CM. The relationship between pH and zeta potential of 30 nm metal oxide nanoparticle suspensions relevant to in vitro toxicological evaluations. Nanotoxicology. 2009; 3:276–283.

Bergman L, Rosenholm J, Öst A-B, Duchanoy A, Kankaanpää P, Heino J, Lindén M. On the complexity of electrostatic suspension stabilization of functionalized silica nanoparticles for biotargeting and imaging applications. J Nanomaterials. 2008:712514.

Deguchi S, Yamazaki T, Mukai S, Usami R, Horikoshi K. Stabilization of C60 nanoparticles by protein adsorption and its implications for toxicity studies. Chem Res Toxicol. 2007; 20:854–858. [PubMed: 17503852]

Deng ZJ, Mortimer G, Schiller T, Musumeci A, Martin D, Minchin RF. Differential plasma protein binding to metal oxide nanoparticles. Nanotechnology. 2009; 20:455101. [PubMed: 19822937]

Dockery DW. Epidemiologic evidence of cardiovascular effects of particulate air pollution. Environ Health Perspect. 2001; 109:483–486. [PubMed: 11544151]

Driscoll KE, Lindenschmidt RC, Maurer JK, Perkins L, Perkins M, Higgins J. Pulmonary response to inhaled silica or titanium dioxide. Toxicol Appl Pharmacol. 1991; 111:201–210. [PubMed: 1659753]

Geiser M, Casaulta M, Kupferschmid B, Schulz H, Semmler-Behnke M, Kreyling W. The role of macrophages in the clearance of inhaled ultrafine titanium dioxide particles. Am J Resp Cell Mol Biol. 2008; 38:371–376.

Gilmour PS, Brown DM, Lindsay TG, Beswick PH, MacNee W, Donaldson K. Adverse health effects of PM10 particles: involvement of iron in generation of hydroxyl radical. Occup Environ Med. 1996; 53:817–822. [PubMed: 8994401]

Gojova A, Guo B, Kota RS, Rutledge JC, Kennedy IM, Barakat AI. Induction of inflammation in vascular endothelial cells by metal oxide nanoparticles: effect of particle composition. Environ Health Perspect. 2007; 115:403–409. [PubMed: 17431490]

Hang J, Shi L, Feng X, Xiao L. Electrostatic and electrosteric stabilization of aqueous suspensions of barite nanoparticles. Powder Technol. 2009; 192:166–170.

Horie M, Nishio K, Fujita K, Endoh S, Miyauchi A, Saito Y, et al. Protein adsorption of ultrafine metal oxide and its influence on cytotoxicity toward cultured cells. Chem Res Toxicol. 2009; 22:543–553. [PubMed: 19216582]

Jeng HA, Swanson J. Toxicity of metal oxide nanoparticles in mammalian cells. J Env Sci Health A. 2006; 41:2699–2711.

Jiang J, Oberdörster G, Biswas P. Characterization of size, surface charge, and agglomeration state of nanoparticle dispersions for toxicological studies. J Nanoparticle Res. 2009; 11:77–89.

Karlsson HL, Cronholm P, Gustafsson J, Möller L. Copper oxide nanoparticles are highly toxic: a comparison between metal oxide nanoparticles and carbon nanotubes. Chem Res Toxicol. 2008; 21:1726–1732. [PubMed: 18710264]

Kosmulski, M. Chemical Properties of Material Surfaces. Marcel Dekker; New York: 2001.

Lin W, Xu Y, Huang CC, Ma Y, Shannon KB, Chen DR, Huang YW. Toxicity of nano- and micro-sized ZnO particles in human lung epithelial cells. J Nanopart Res. 2009; 11:25–39.

Linse S, Cabaleiro-Lago C, Xue W-F, Lynch I, Lindman S, Thulin E, et al. Nucleation of protein fibrillation by nanoparticles. Proc Nat Acad Sci. 2007; 104:8691–8696. [PubMed: 17485668]

Luik AI, Naboka YN, Mogilevich SE, Hushcha TO, Mischenko NI. Study of human serum albumin structure by dynamic light scattering: two types of reactions under different pH and interaction with physiologically active compounds. Spectrochim Acta A. 1998; 54:1503–1507.

Lynch I, Dawson KA. Protein-nanoparticle interactions. NanoToday. 2008; 3:40–47.

Meißner T, Potthoff A, Richter V. Suspension characterization as important key for toxicological investigations. J Phys Conf Ser. 2009; 170:012012.

Moreau JW, Weber PK, Martin MC, Gilbert B, Hutcheon ID, Branfield JF. Extracellular proteins limit the dispersal of biogenic nanoparticles. Science. 2007; 316:1600–1603. [PubMed: 17569859]

Nemmar A, Vanbilloen H, Hoylaerts MF, Hoet PHM, Verbruggen A, Nemery B. Passage of intratracheally instilled ultrafine particles from the lung into the systemic circulation in hamster. Am J Resp Crit Care Med. 2001; 164:1665–1668. [PubMed: 11719307]

Norde W, Giacomelli CE. BSA structural changes during homo-molecular exchange between the adsorbed and the dissolved states. J Biotech. 2000; 79:259–268.

Nurkiewicz TR, Porter DW, Hubbs AF, Stone S, Chen BT, Frazer DG, et al. Pulmonary nanoparticle exposure disrupts systemic microvascular nitric oxide signaling. Toxicol Sci. 2009; 110:191–203. [PubMed: 19270016]

Oberdörster G, Sharp Z, Atudorei V, Elder A, Gelein R, Lunts A, et al. Extrapulmonary translocation of ultrafine carbon particles following whole-body inhalation exposure of rats. J Toxicol Environ Health A. 2002; 65:1531–1543. [PubMed: 12396867]

Patil S, Sandberg A, Heckert E, Self W, Seal S. Protein adsorption and cellular uptake of cerium oxide nanoparticles as a function of zeta potential. Biomaterials. 2007; 28:4600–4607. [PubMed: 17675227]

Pratten MK, Lloyd JB. Pinocytosis and phagocytosis: the effect of size of a particulate substrate on its mode of capture by rat peritoneal macrophages cultured in vitro. Biochim Biophys Acta. 1986; 881:307–313. [PubMed: 3008849]

Rezwan K, Meier LP, Rezwan M, Vörös J, Textor M, Gauckler LJ. Bovine serum albumin adsorption onto colloidal Al2O3 particles: a new model based on zeta potential and UV-vis measurements. Langmuir. 2004; 20:10055–10061. [PubMed: 15518493]

Schulze C, Kroll A, Lehr CM, Schäfer UF, Becker K, Schnekenburger J, et al. Not ready to use—overcoming pitfalls when dispersing nanoparticles in physiological media. Nanotoxicology. 2008; 2:51–61.

Thomassen LCJ, Aerts A, Rabolli V, Lison D, Gonzalez L, Kirsch-Volders M, et al. Synthesis and characterization of stable monodisperse silica nanoparticle sols for in vitro cytotoxicity testing. Langmuir. 2010; 26:328–335. [PubMed: 19697952]

Tolpekin VA, Duits MHG, van den Ende D, Mellema J. Aggregation and breakup of colloidal particle aggregates in shear flow, studied by video microscopy. Langmuir. 2004; 20:2614–2627. [PubMed: 15838950]

Vamanu CI, Høl PJ, Allouni ZE, Elsayed S, Gjerdet NR. Formation of potential titanium antigens based on protein binding to titanium dioxide nanoparticles. Int J Nanomedicine. 2008; 3:69–74. [PubMed: 18488417]

Wu W, Sun X, Yu Y, Hu J, Zhao L, Liu Q, et al. $TiO_2$ particles promote b-amyloid fibrillation in vitro. Biochem Biophys Res Comm. 2008; 373:315–318. [PubMed: 18571499]

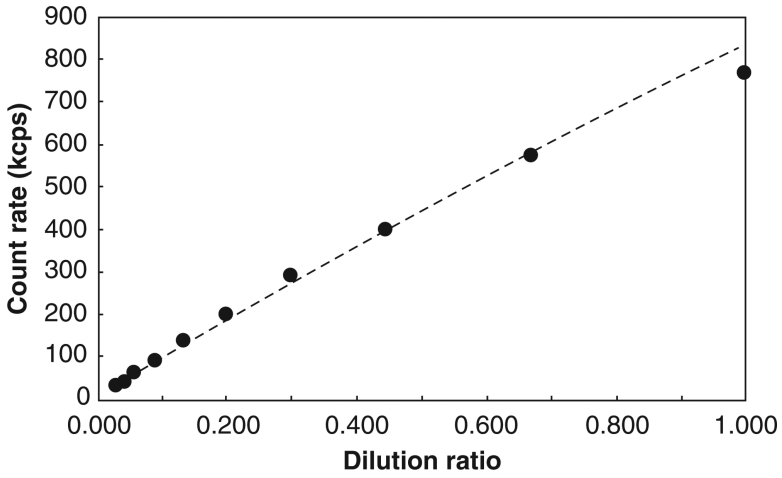


**Figure 1.**
Validation of the count rate method. Count rate variation with particle concentration to the power of 0.91 correlates extremely well with the data ($r^2 > 0.999$).

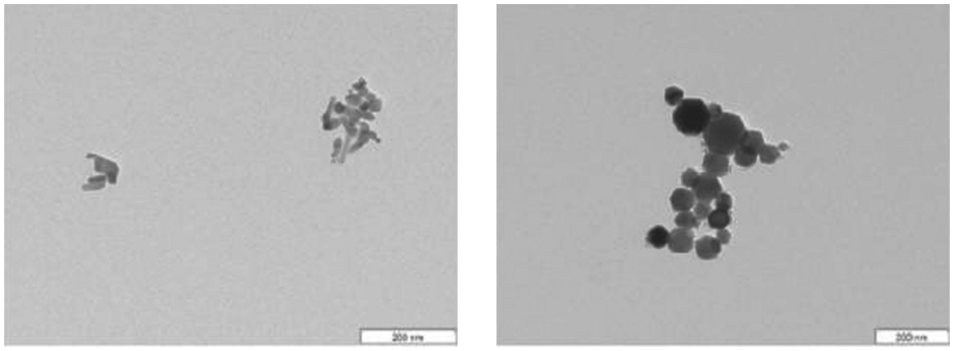

**Figure 2.**
TEM images of iron oxide (right) and zinc oxide (left) nanoparticle aggregates.

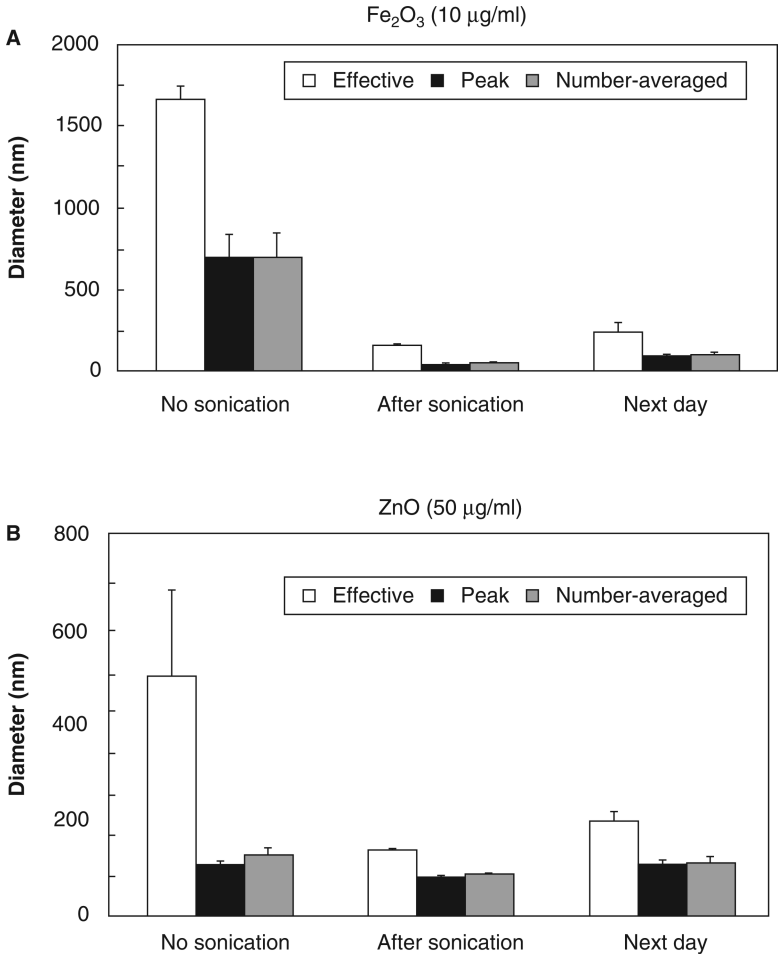


**Figure 3.**

Dispersion and recovery of metal oxide nanoparticles. Each measure was calculated independently for each of six trials and then averaged. Data are mean ± SEM. (A) Iron oxide (10 μg/ml). (B) Zinc oxide (50 μg/ml).

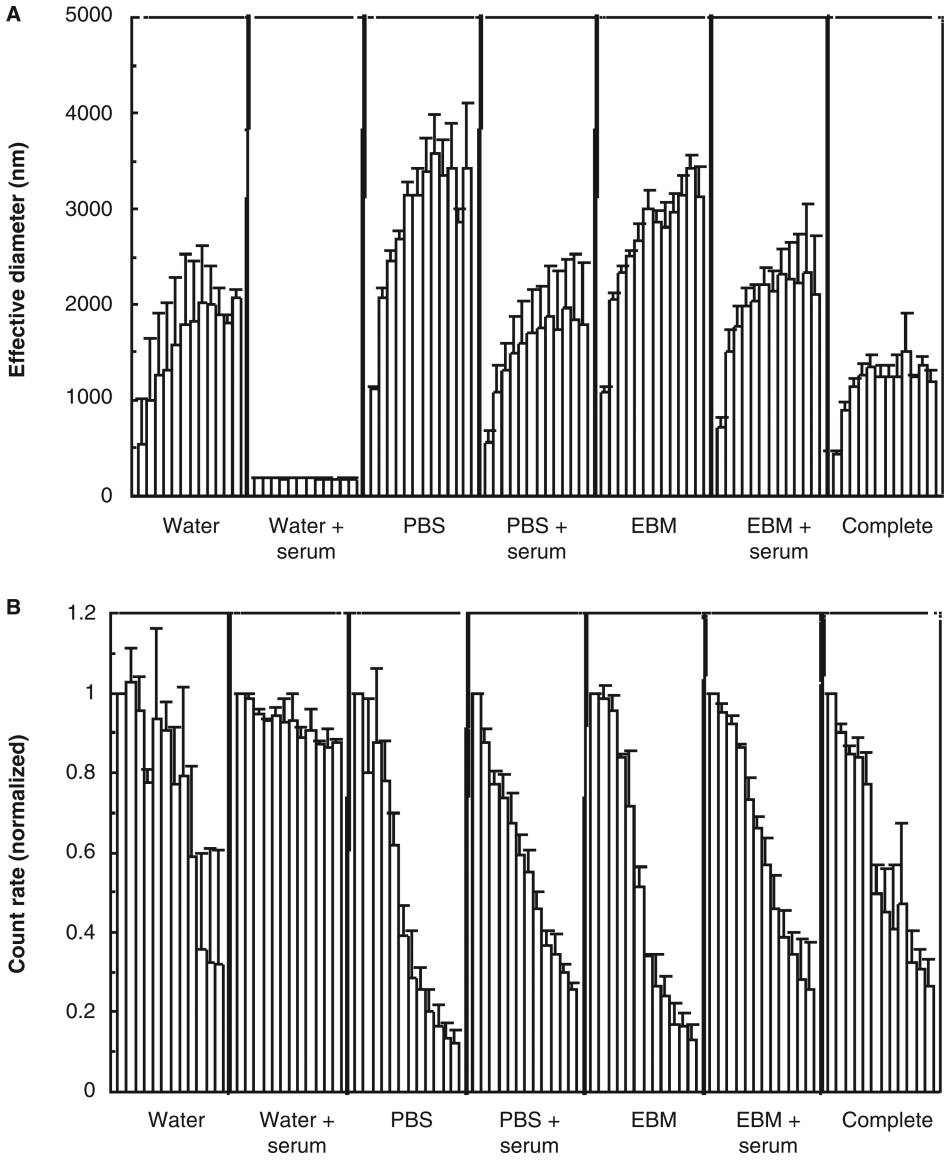


**Figure 4.**

Short-term aging of iron oxide nanoparticles. (A) Particle size. (B) Scattering intensity. Measured values from three replicates were averaged at each 1-h time step. Data are mean ± SEM.

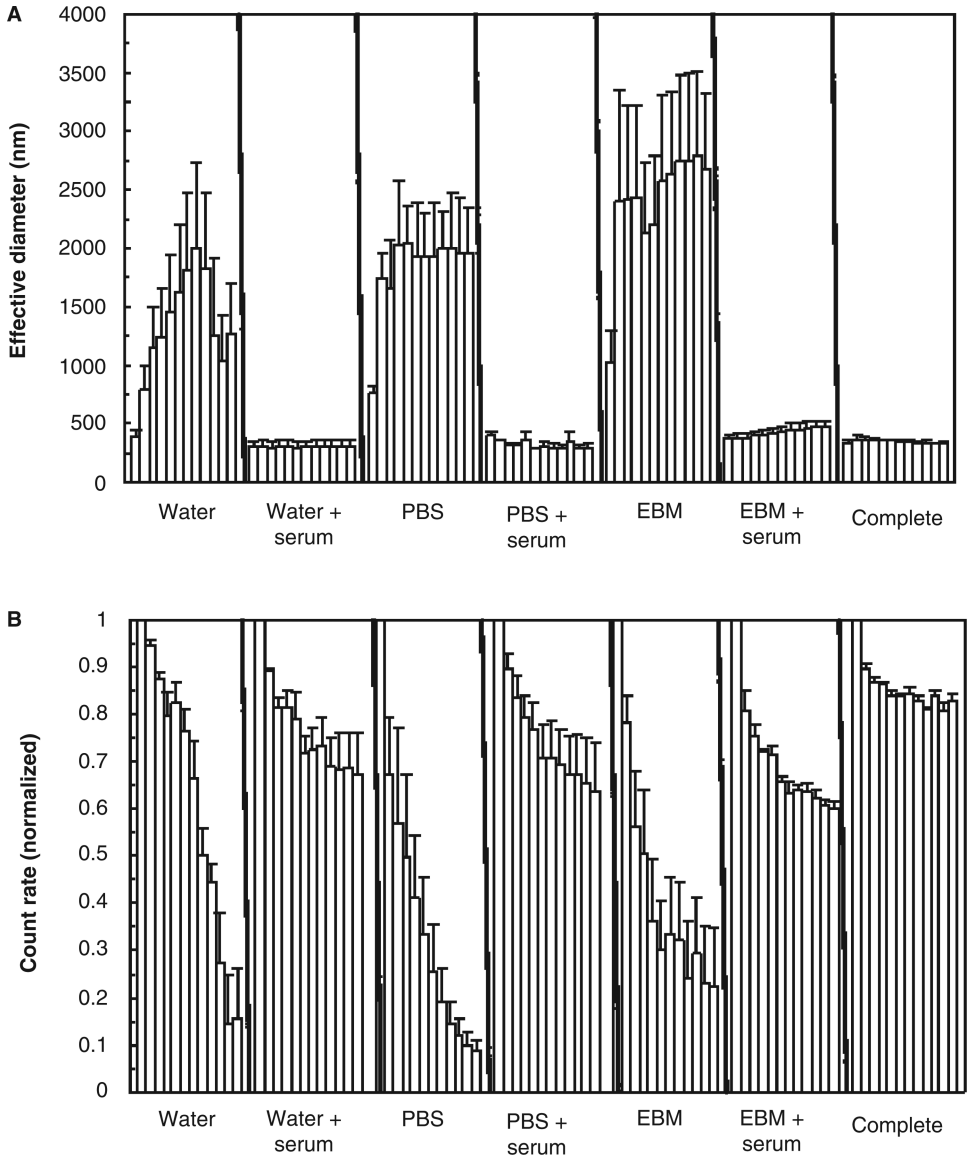


**Figure 5.**

Short-term aging of zinc oxide nanoparticles. (A) Particle size. (B) Scattering intensity. Measured values from three replicates were averaged at each 1-h time step. Data are mean ± SEM.

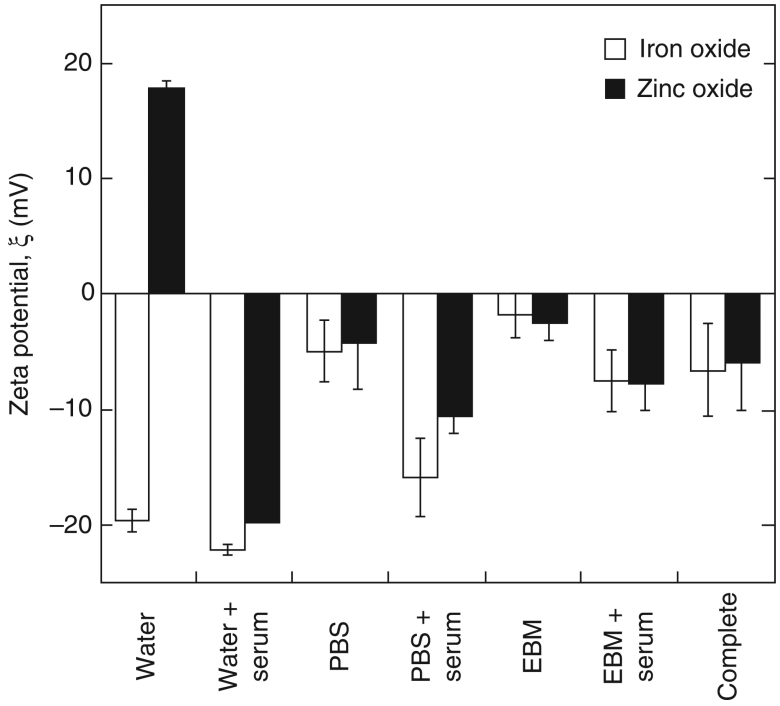


**Figure 6.**
Effect of serum on zeta potential in various diluents for iron oxide and zinc oxide nanoparticles. Each data point is the average of three experiments. Data are mean ± SEM.

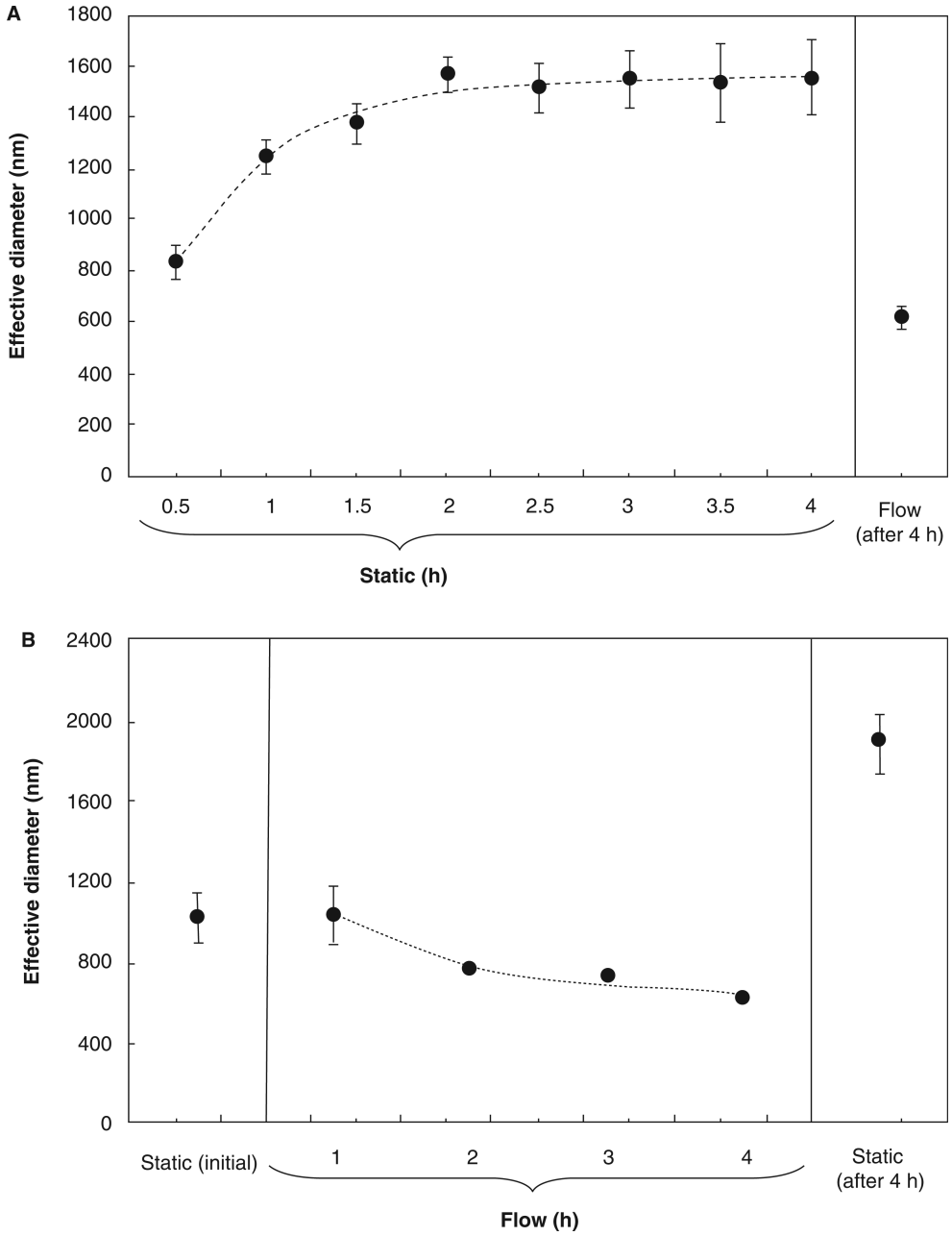


**Figure 7.**

Effect of flow on aggregation of iron oxide nanoparticles in complete medium. (A) Evolution of particle diameter over 4 h under static conditions. Also shown is particle diameter under flow conditions at the end of the 4-h period. Data are mean ± SEM with $n$ = 4. (B) Evolution of particle diameter over 4 h under flow conditions. Also shown are particle diameters under static conditions at the beginning and end of the 4-h period. Data are mean ± SEM with $n$ = 2.

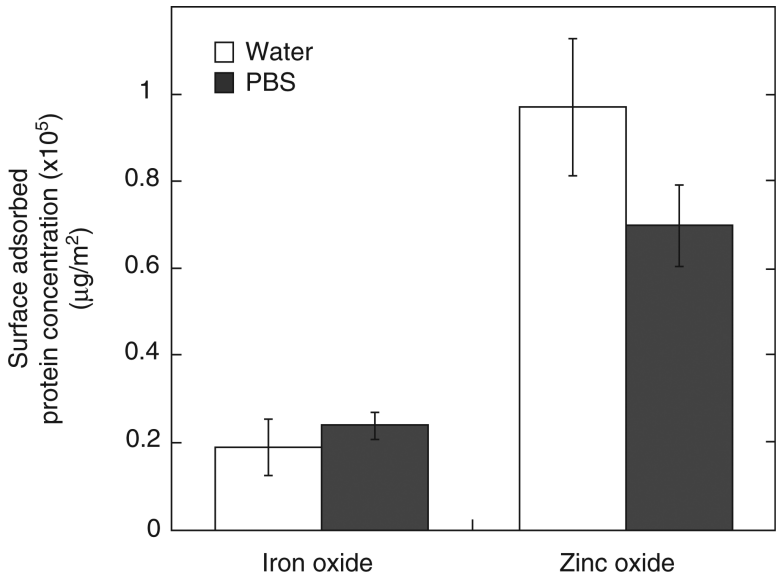


**Figure 8.**
Concentration of protein, normalised by specific surface area, adsorbed on iron oxide and zinc oxide nanoparticles in DI water and PBS diluents. Data are mean ± SEM with $n = 3$.

## Table I

Aging results at 12 h.

| | | Water | | PBS | | EBM | | |
|---|---|---|---|---|---|---|---|---|
| | **Serum** | **–** | **+** | **–** | **+** | **–** | **+** | **Complete medium** |
| $Fe_2O_3$ | ED (nm) | 1866 | 180 | 2282 | 1495 | 2444 | 1783 | 1054 |
| | CR% | 26.9% | 87.9% | 7.2% | 22.3% | 8.0% | 22.9% | 23.9% |
| ZnO | ED (nm) | 1759 | 307 | 1956 | 285 | 2679 | 470 | 329 |
| | CR% | 2.8% | 67.4% | 9.0% | 63.6% | 22.5% | 60.2% | 83.0% |

CR%: count rate as a percentage of the value measured in the first hour; EBM: endothelial cell basal medium-2; ED: effective diameter (nm); PBS: phosphate buffered saline; ZnO: zinc oxide.